Longitudinal grey-box model identification of a tailless flapping wing mav based on free-flight data

Nijboer, J. B.W.; Armanini, S. F.; Karásek, M.; de Visser, C. C.

DOI
10.2514/6.2020-1964

Publication date
2020

Document Version
Final published version

Published in
AIAA Scitech 2020 Forum

AIAA SciTech Forum
6-10 January 2020, Orlando, FL
AIAA Scitech 2020 Forum

10.2514/6.2020-1964

Longitudinal Grey-Box Model Identification of a Tailless Flapping Wing MAV Based on Free-Flight Data

J.B.W Nijboer*
Delft University of Technology, Delft, Zuid-Holland, 2629 HS

S.F. Armanini †
Imperial College London, London, South Kensington, SW7 2AZ

M. Karásek‡ and C.C. de Visser§
Delft University of Technology, Delft, Zuid-Holland, 2629 HS

Tailless flapping wing micro aerial vehicles (FMWAVs) are known for their light weight and agility. However, given the fact that these FWMAVs have been developed only recently, their flight dynamics have not yet been fully explained. In this paper we develop grey-box models for the time-averaged longitudinal dynamics of a tailless FWMAV (DelFly Nimble) from free-flight data using closed-loop system identification techniques. The consequence of the tailless configuration is inherent instability, therefore tailless FWMAVs are generally more complex than their tailed counterparts and require an active feedback control system. The control system introduces additional challenges to the system identification process as it counteracts the perturbations required to excite the system. Based on this approach, grey-box models were estimated and validated for airspeeds ranging from hover conditions, 0 m/s, to 1.0 m/s forward flight. Despite the complexity of the system, we were able to obtain low-order local models that are both efficient and accurate (R^2 values up to 0.92) and can therefore be used for stability analysis, simulation and control design. With these models we can also take the first steps towards fully understanding the flight dynamics of tailless FWMAVs.

Nomenclature

δ_D	=	Control deflection. Measured dihedral deflection
r	=	Reference signal of closed-loop automatic feedback system
e	=	Error signal of closed-loop automatic feedback system
u	=	Controller output signal of closed-loop automatic feedback system
y	=	System output
y_m	=	Measured system output
x, y, z	=	Position
q_0, q_1, q_2, q_3	=	Attitude quaternions
p	=	Roll rate
q	=	Pitch rate
r	=	Yaw rate
$\dot{p}$	=	Roll acceleration
$\dot{q}$	=	Pitch acceleration
$\dot{p}$	=	Yaw acceleration
a_x	=	Linear acceleration in x-direction
a_y	=	Linear acceleration in y-direction
a_z	=	Linear acceleration in z-direction
θ_{sp}	=	Pitch attitude angle set-point

*M.Sc. Graduate Student, Faculty of Aerospace Engineering, Department of Control & Simulation, jorgen.nijboer@gmail.com
†Research Associate, Faculty of Engineering, Department of Aeronautics, s.armanini@imperial.ac.uk
‡Guest Researcher, Faculty of Aerospace Engineering, Department of Control & Simulation, m.karasek@tudelft.nl
§Assistant Professor, Faculty of Aerospace Engineering, Department of Control & Simulation, c.c.devisser@tudelft.nl

f_{flap}	=	Flapping frequency
θ_{ref}	=	Pitch angle reference
$\dot{\theta}_{ref}$	=	Pitch rate reference
θ_m	=	Measured pitch angle
$\dot{\theta}_m$	=	Measured pitch rate
K_D	=	Rate feedback gain
K_P	=	Attitude feedback gain
X	=	Measured aerodynamic force in x-direction
Z	=	Measured aerodynamic force in z-direction
M	=	Measured aerodynamic moment around the y-axis
m	=	Mass
g	=	Gravitational acceleration
u	=	Velocity along the body x-axis
v	=	Velocity along the body y-axis
w	=	Velocity along the body z-axis
$\dot{u}$	=	Acceleration along the body x-axis
$\dot{w}$	=	Acceleration along the body z-axis
θ	=	Pitch angle
θ_0	=	Trimmed pitch angle
ϕ	=	Roll angle
ψ	=	Yaw angle
α	=	Angle of attack
I_{xx}, I_{yy}, I_{zz}, I_{xz}	=	Moments of inertia of a 3D body
X_q, X_u, X_w, X_{δ_D}	=	Longitudinal-directional derivatives
Z_q, Z_u, Z_w, Z_{δ_D},Z_0, Z_{qu}	=	Longitudinal-directional derivatives
Z_{w^2}, Z_{u^2}, $Z_{\delta_D w}$, $Z_{\delta_D q}$, Z_{q^2}	=	Longitudinal-directional derivatives
M_q, M_u, M_w, M_{δ_D}	=	Longitudinal-directional derivatives
Δ	=	Perturbation of corresponding variable
$b_{\dot{q}}$	=	Bias terms of the grey-box state-space system
$\mathbf{X}$	=	Regression matrix
$\mathbf{z}$	=	Vector of measured output OLS estimator
$\boldsymbol{\theta}$	=	Vector containing model parameters
$\hat{\theta}$	=	Vector with the best estimators for $\boldsymbol{\theta}$
$\boldsymbol{\epsilon}$	=	Model residuals vector
$\mathbf{J}(\boldsymbol{\theta})$	=	Cost function J as a function of the vector containing model parameters
$\hat{\sigma}$	=	Estimated standard deviation
R^2	=	Coefficient of determination (goodness of fit)

I. Introduction

Unmanned aerial vehicles have proven to be very valuable for both the civil and the military sectors. The ever growing demand for these vehicles has also motivated designers to explore unconventional implementations [1, 2]. An example of this is the biologically inspired Flapping-Wing Micro Aerial Vehicle (FWMAV). FWMAVs are typically very lightweight and capable of performing rapid manoeuvres, meaning they are very agile at both hover and high-speed conditions [3–6]. Given these favourable properties, the demand for FWMAVs is expected to grow in the near future, and many useful applications can be envisaged, e.g. surveillance within buildings where high manoeuvrability is essential. Among FWMAVs, tailless vehicles stand out for their high agility compared to tailed ones, however they are inherently unstable and require an active control system for stabilization [7, 8]. They are also typically more complex, with actuation provided solely via the wings. Examples of successful tailless FWMAVs are the Nano Hummingbird, the bio-inspired Colibri and the KUBeetle [5, 9–11].

An attractive approach for modelling FWMAVs is the use of low-order dynamic models based on the Equations of Motion (EOM) of a conventional rigid-body aircraft [8, 12–16]. These models are typically flap cycle-averaged and sometimes linearized. They are therefore relatively simple and computationally efficient, hence useful for practical applications. One approach to obtain simple yet accurate dynamic models is free-flight system identification, often

based on motion tracking data. This approach has been applied previously to tailed FWMAVs and the resulting grey-box models have been found to be sufficiently accurate for stability analysis, control system design and simulation [12, 17]. Modelling work on tailless FWMAVs, however, is relatively scarce. Roshanbin et al used a simple linear model that captures the longitudinal pitch dynamics, with parameters estimated using pendulum experiments [10]. In addition, a minimal longitudinal dynamic non-linear model has recently been devised[18] for the DelFly Nimble, a bio-inspired tailless FWMAV developed at Delft University of Technology (Figure 1) [3]. The non-linear model is developed using an output error approach where the unknown aerodynamic damping coefficients are identified based on optimization routines that minimizes the square of the residuals between the simulation output and free-flight OptiTrack-recorded data. The research of K.M. Kajak et al does not include the use of a standard aircraft system identification technique. Rather K.M. Kajak et al developed a physically derived non-linear model in which the identified parameters are aerodynamic damping coefficients and lengths. Although non-linear models of the Nimble have been developed in a previous study [18], this study focuses on identifying linear models using a more structured aircraft system identification approach, where the estimated parameters are longitudinal-directional aerodynamic derivatives (stability- and control derivatives). These derivatives effectively provide information regarding how much change occurs in the aerodynamic- forces and moments acting on the DelFly Nimble when there is a small change in states and control surfaces deflection. As a result, the stability of the DelFly Nimble can be readily analysed using these estimated control- and stability derivatives.

Although standard aircraft system identification approaches have been applied successfully to tailed (stable) FWMAVs, they have not yet been applied to tailless FWMAV stabilized and controlled in closed loop.

In this work, we test the feasibility of using standard aircraft system identification techniques to identify grey-box longitudinal models of an inherently unstable tailless FWMAV (DelFly Nimble). An additional goal was to obtain models well-suited for stability analysis, simulation and control design purposes. Hence, the models should be accurate, computationally efficient and relatively simple, especially if intended for on-board use. Like other tailless FWMAVs, the unstable DelFly Nimble needs to be stabilized and controlled by means of active rate and attitude feedback control on its wing actuation system, in order to maintain controlled flight. Instability brings additional challenges when applying open-loop system identification techniques, as performing open-loop flight tests is not possible. In closed-loop flight experiments it was found to be challenging to ensure reproducible test conditions, especially when performing identification manoeuvres manually. By performing flight experiments manually, the quality of the experiments relied heavily on the handling capabilities of the pilot and as a consequence, varied almost each flight. In order to improve repeatability we therefore used automated manoeuvres, activated once the test platform was trimmed in the desired flight condition. An additional and related challenge lies in acquiring informative flight data, i.e. data suitable for system identification. While motion tracking was found to provide sufficiently accurate and informative data in free-flight experiments on the DelFly Nimble, it was a greater challenge to perform manoeuvres that sufficiently excite the natural motions of the FWMAV within the practical boundaries of the flight testing. A further difficulty is that the natural motions are damped or even eliminated by the active feedback system, which negatively impacts the information content of the data.

Applying the aforementioned closed-loop system identification approach, we obtained cycle-averaged models for the flight dynamics of the DelFly Nimble. The resulting low-order grey-box models accurately describe the FWMAV's time-averaged behaviour in flight conditions ranging from hover- (0.0 m/s) up to forward flight (1.0 m/s) conditions, and are of a low order and computationally efficient. Hence they can be used for simulation and stability analysis. While simple, they still provide insight into the flight dynamics of the DelFly Nimble and serve as a tool for the development of new advanced controllers. The models are estimated and validated using free-flight data obtained from optical tracking devices. Based on the results, we can conclude that system identification techniques can effectively be applied to tailless FWMAVs, resulting in both computationally efficient and accurate models.

This paper is divided into the following sections. In **Section II** the working principles of the DelFly Nimble are discussed together with the experiment set-up. **Section III** explains the model structure, the modelling process and the estimation techniques applied to estimate the unknown model parameters. **Section IV** focuses on the modelling results. And lastly, **Section V** discusses the conclusions of this work and provides recommendations for follow-up studies.

II. Experiment Set-up

In this work, longitudinal grey-box model identification was performed on the DelFly Nimble (Figure 1). The DelFy Nimble is a bio-inspired tailless FWMAV developed at the faculty of Aerospace Engineering of Delft University of Technology [3]. With a wingspan of only 33 cm, the DelFly Nimble is a fairly small platform weighing just under 29 grams (Figure 1). The left and right flapping mechanisms generate thrust depending on the flapping frequency and are

indicated by the red arrows/vectors in Figure **1. A**. The higher the flapping frequency, the higher the produced thrust. The platform includes two servos for yaw and pitch control. The yaw is controlled by changing the vector of the two wings on opposite sides (Figure **1. E, H**). Pitch control is accomplished by changing the dihedral of the flapping-wing mechanisms, thereby changing the location of the thrust vectors with respect to the center of mass (Figure **1. F, I**). As a result, a pitch torque is produced, which rotates the platform to establish forward flight (Figure **1. C**). Roll control is accomplished by differential control of right wing-pair and left wing-pair (Figure **1. G, J**). Since the thrust increases with the flapping frequency, increasing the flapping frequency of one wing and reducing the flapping frequency of the other will generate a differential thrust and therefore roll torque enabling sideways flight (Figure **1. D**).

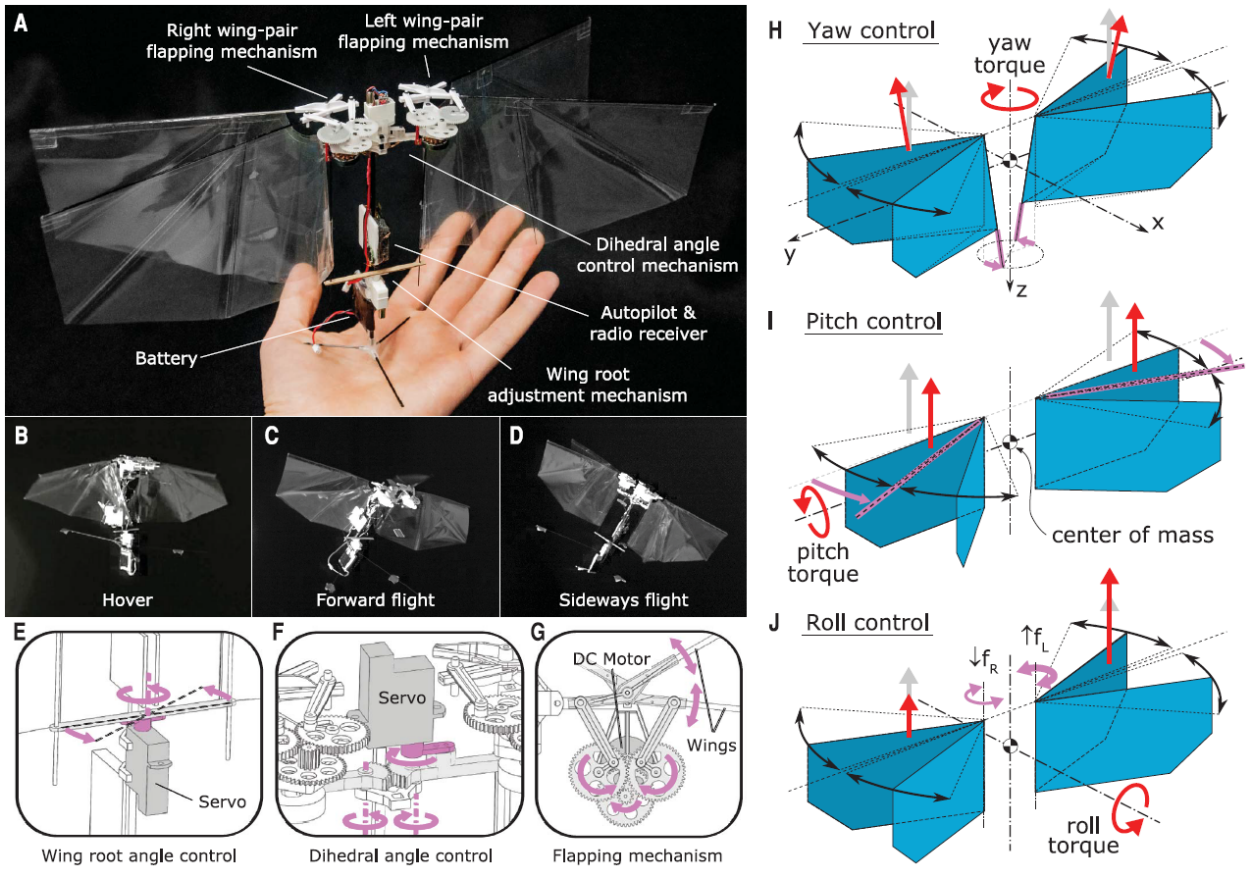

Fig. 1 The DelFly Nimble is controlled by its two flapping mechanisms and control servos. Source: [3]

The system (DeFly Nimble) was identified using a standard system identification approach [19]. The complete system identification cycle typically includes the set-up and automated execution of the flight test experiments (manoeuvres), measurement of the system states and data compatibility/ data processing, reconstruction of the aerodynamic forces and moments, model structure definition, parameter estimation, and evaluation and validation of the modelling results.

Performing system identification on an FWMAV that is stabilized by an automatic feedback control system represents a significant challenge. The objective of performing flight tests (manoeuvres) is to excite the natural dynamics of the FWMAV as much as possible. However, when performing such flight tests the control system regards the natural system responses to manoeuvre inputs as a disturbance and acts to minimize them [19]. While closed-loop system identification techniques have been developed for such cases [20], we opted to use simpler open-loop identification techniques. These have been proven to be applicable as long as the control surface positions δ and system outputs y in **Block-diagram 1** can be measured, and the gains of the feedback system can be reduced such that the natural responses are not completely suppressed [19]. In this work, both δ and y were measurable, hence using an open-loop identification procedure was viable. Markers mounted on the flapping-mechanisms of the DelFly Nimble, together with the recorded on-board servo position, made it possible to measure the dihedral angle which was used as input (δ_D).

This section will additionally explain the in-flight data acquisition process (**Subsection II.A**), the controller

architecture of the Nimble **(Subsection II.B)**, the coordinate frame used for system identification **(Subsection II.C)**, the flight tests required and performed for exciting the natural dynamics of the DelFly Nimble **(Subsection IV)**, and the in-flight data processing **(Subsection II.E)**.

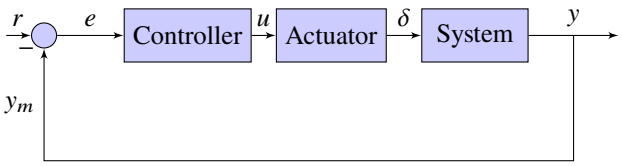

Block-diagram 1: *Basic closed-loop automatic feedback control system.*

A. In-Flight Data Acquisition

In order to obtain in-flight data for system identification, we used an OptiTrack Motion Capture System, installed in the 10m x 10m x 7m flight testing facility of the Delft University of Technology, called the CyberZoo. The system consists of 12 Prime 17W OptiTrack cameras that provide high-resolution measurements of both the position and the orientation of a body fitted with retro-reflective markers at a rate of up to 360 Hz. During the in-flight data acquisition phase data was captured at a rate of 200 Hz. A total of six retro-reflective markers, made from 20 mm styrofoam balls covered with retro-reflective material, were mounted on the DelFly Nimble in order to determine the position, orientation of the body in the OptiTrack environment as well as the dihedral deflection (δ_D). In addition to the OptiTrack measurements, on-board measurements were obtained from the 1.5 g Lisa MXS autopilot. Radio control set point, controller outputs and servo positions were recorded on a micro-SD card at a rate of approximately 100 Hz. Refer to Table 1 for an overview of all the data obtained and by which data acquisition system they were provided.

Type sensor	**Measurements obtained**
OptiTrack	Position (x,y,z)
	Attitude quaternions (q_0, q_1, q_2, q_3)
	Control deflections (δ_D)
IMU AHRS	Angular velocities (p,q,r)
	Linear accelerations (a_x, a_y, a_z)
On-board extra	Flap frequency (f_{flap})
	Set-point (θ_{sp})
	Dihedral command (cmd_{pitch})
	Servo feedback ($dihedral_{feedback}$)

Table 1 Data provided by data acquisition systems during flight tests.

B. Controller Architecture

The DelFly Nimble is stabilized by a fixed-gain parallel feedback controller with attitude and rate feedback [3]. A command filter, which is a low-pass filter with a cut-off frequency of 15 Hz, was added to the controller in order to reduce the noise generated by vibrations of the fuselage (as a result of the unsynchronyzed flapping mechanisms) and improve delays introduced into the control loop [3]. In manual flight mode, the pilot provides an attitude set-point via the remote controller (RC). Alternatively, a sequence of attitude set-points can be pre-programmed and triggered in flight, which is what was used for the system identification maneuvers. In both cases, the reference generator will then generate the reference attitude and rate. The controller architecture can be found in Figure 2.

C. Coordinate Frame Definition

The frame used for system identification is defined as follows: the body X-axis is pointing forward, the body Y-axis is pointing to the right and the body Z-axis is pointing downward (refer to Figure **1. H**). In addition, the positive inertial X-axis and Z-axis are pointing forward and downward, respectively (Figure 3). This coordinate frame was used in order

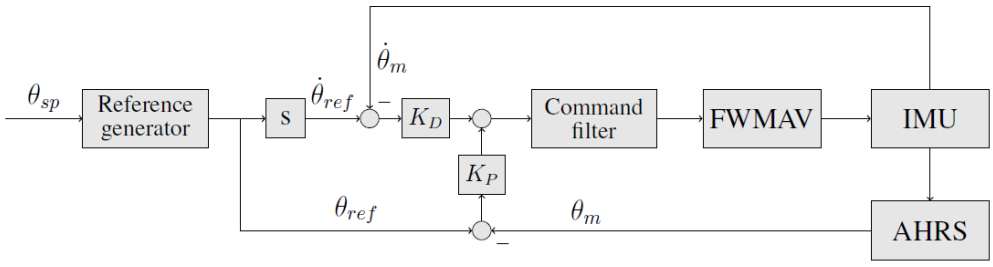

Fig. 2 Controller architecture. The set-point is denoted by subscript sp, the reference by ref and the measurement by m. Source: [18]

to prevent singularity issues when performing manoeuvres in hover and forward flight. Note that the X_{body} axis in Figure **3** coincides with the X-axis in Figure **1. H**. The same holds for the Z-axis.

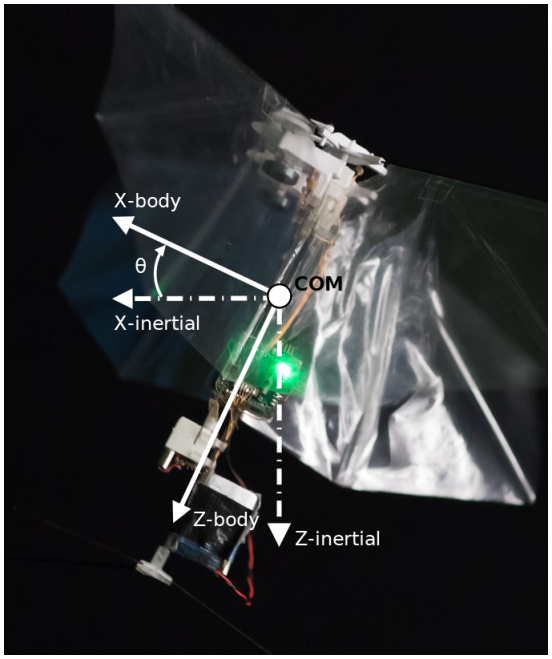

Fig. 3 Longitudinal free body diagram of the DelFly Nimble. Positive angles for θ are defined by clockwise rotation.

D. Flight Tests Required for System Identification

Important factors that affect the quality of the modelling and system identification process are data acquisition and data processing. However, the flight testing, which includes the input signal applied to the system to be identified, is especially important. The input signals need to excite the natural dynamics of the system, providing useful and informative data in the frequency range of interest. In this work, the manoeuvres were designed based on existing input design theory, the constraints associated with the experimental set-up (e.g. the dimensions of the CyberZoo), the test platform itself and past experience with similar robots [21, 22].

For input design it is typical to use a priori knowledge of the system at hand if available, however, in the case of the DelFly Nimble, a priori information was limited. Another approach is to use frequency sweep inputs, exciting as many frequencies as possible. The drawback of frequency sweeps is the relatively long time they take to perform, especially when covering a wide range of frequencies. Due to the long manoeuvre duration, the limited flight space available

hinders the flight testing. As a compromise between execution time and frequency coverage, doublet inputs were applied in this study. Although doublets cover a narrower frequency range than frequency sweeps, they are advantageous to use due to the limited flight testing space they require and the fact that the FWMAV is more likely to remain in its initial steady flight condition since the manoeuvre is symmetrical. The latter point is especially important when using linearised model structures. Previous studies on modelling FWMAV dynamics also found that doublets provided adequate excitation [21, 22].

Hence, to model the longitudinal dynamics of the DelFly Nimble we applied doublet inputs to the pitch command in closed-loop operation. Since the feedback gains dampen the natural dynamic response of the vehicle we weakened the original feedback gains. Based on previous studies on the DelFly Nimble [18] we were able to gain insight into the dynamic response of the robot with changing feedback gains and adjusted the gain settings accordingly (Table 2).

Original gains	**Adjusted gains for system identification**
$K_P = 1.6250$	$K_P = 2.0833$
$K_D = 0.20832$	$K_D = 0.0500$

Table 2 The adjust gain settings were used for system identification flight tests.

Automated manoeuvres were performed to ensure repeatability and consistency during each flight test. These manoeuvres were tuned in (a) input duration, (b) input amplitude and (c) input type (selection of actuators) in order to improve the excitation of the natural dynamic response of the system. When the automated manoeuvre is activated it sends a doublet attitude reference set-point (θ_{sp}) to the reference generator as seen in Figure 2. As a result, the DeFly Nimble will perform a doublet manoeuvre while remaining in closed-loop operation. Figure 4 shows an example of a typical automated manoeuvre performed for system identification, where the set-point is θ_{sp} and the measured dihedral δ_D is the input that goes directly into the FWMAV.

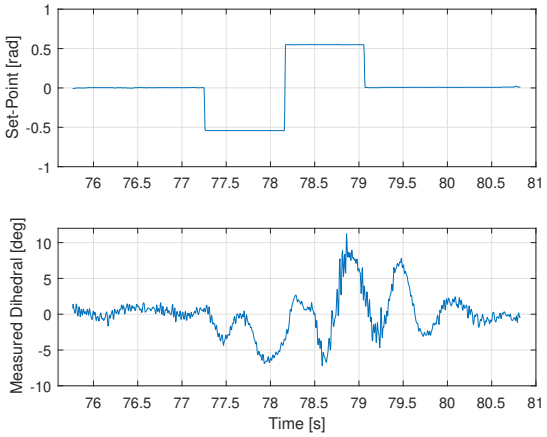

Fig. 4 Typical set-point θ_{sp} signal sent to the reference generator, including the corresponding measured dihedral δ_D used for model identification of the DelFly Nimble.

E. Data Acquisition and Processing

The OptiTrack motion tracking system was selected as the primary data acquisition system to derive all the states required for system identification. Other studies have proven that motion tracking data-based system identification can lead to sufficiently accurate models [12, 23]. While IMU sensor readings yield a higher resolution (approximately 512 Hz) compared to OptiTrack ones (360 Hz), such high resolution is only important when accurate analysis is required at a sub flap-cycle time scale [24]. For the purpose of modelling cycle-averaged flight dynamics, the refresh rate of 360 Hz of the OptiTrack system is therefore considered adequate [12]. In addition to the tracking data, on-board data, such as the motor speed, was recorded on an SD-card at a rate of approximately 100 Hz [18].

Based on previous studies, a third-order zero-phase Butterworth filter was used to filter the raw data [13]. First a cutoff frequency of 50 Hz was used to remove the noise. The cutoff frequency was chosen based on frequency domain analysis of the flight data, in which after the 2^{nd} harmonic the data is considered as noise (Figure 5). Next, based on the assumption that the body and flapping dynamics are decoupled, we averaged out the data over the flap cycle in order to remove time-varying effects. There is some discussion suggesting that it is not always justified to cancel out the time-varying effects [25], however this remains the most common and accepted approach when modelling FWMAV dynamics [12, 15]. The Power Spectral Density (PSD) plot of the raw acceleration measured in z-direction, shown in Figure 5, clearly displays two peaks. The first represents mainly the flapping frequency, which is around 16 Hz, and the successive one represent the flapping harmonic. Filtering the data below these frequencies will remove the time-varying effects. Based on previous research [12, 18], a cut-off frequency of 5 Hz was used to filter out the time-varying effects, and thereby making sure only the body dynamics are preserved in the data.

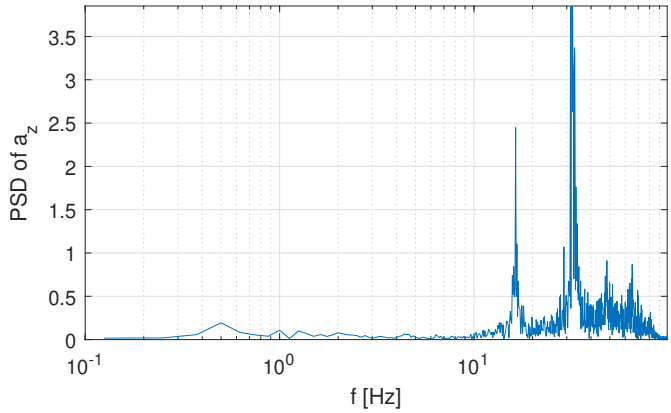

Fig. 5 Power spectrum density (PSD) of the acceleration in z-direction a_z derived from OptiTrack data.

The OptiTrack system only provides information on the position and orientation of the FWMAV. However, in order to derive other states essential for system identification, such as velocity and pitch rate, we must use an appropriate differentiation scheme to derive these states as accurately as possible. Based on the study by Caetano et al [23], who studied the effects of numerical differentiation on free-flight data obtained for a FWMAV, we chose a three point central difference (Equation 1) for numerical differentiation, as it reduces error amplification significantly compared to other methods and will not result in time lags or significant smoothing. All states were then derived from the position- and orientation data by applying Equation 1.

$$\dot{x}_t = \frac{x_{t+1} - x_{t-1}}{2\Delta t} \tag{1}$$

III. Model Structure Definition and Parameter Estimation

In **Section III.A** a comprehensive explanation of the chosen model structure will be provided. The following step is to estimate the unknown parameters in the chosen model structure using the free-flight data obtained from the flight tests . This will be explained in **Section III.B**.

A. Model Structure Determination and Definition

A grey-box system identification approach was used to model the dynamics of the DelFly Nimble, based on research by Armanini et al [12]. Grey-box identification allows for available a priori knowledge of the system dynamics to be included in the model structure, maintaining a connection to the physics of the system. Measured data can then be used to determine the unknown parameters in the model structure. If the model structure and data are appropriate, the result will be an accurate model validated with real data, and still maintaining a connection to the physics of the system being modelled. The time-averaged dynamics of the DelFly Nimble were modelled based on the Equations of motion (EOM) of a conventional fixed-wing rigid-body aircraft (Equations 2a-2c), shown below for the variables relevant for

the longitudinal dynamics.

Aerodynamic force Equations:

$$\begin{aligned} X &= m(\dot{u} + g\sin\theta - rv + qw) \\ Z &= m(\dot{w} - g\cos\theta\cos\phi - qu + pv) \end{aligned} \tag{2a}$$

Aerodynamic moment Equation:

$$M = \dot{q}I_{yy} + rp(I_{xx} - I_{zz}) - (p^2 + r^2)I_{xz} \tag{2b}$$

Kinematic Equation:

$$\dot{\theta} = q\cos\phi - r\sin\phi \tag{2c}$$

Although the DelFly Nimble does not resemble a conventional aircraft, previous studies have shown that these EOM can describe the motion of some flapping-wing flyers [23, 26–28]. In addition, we do not know the dynamics of the DelFly Nimble very well yet, therefore the use of standard aircraft EOM is a logical first step. The EOM (Equations 2a-2c) were linearised around a forward flight trimmed condition and decoupled to only include the longitudinal terms.

The next step was to assume a linear model structure for the aerodynamic forces and moments incorporated in the EOM. Aerodynamic models used for fixed-wing aircraft are typically linear-in-the-parameters, as this simplifies the parameter estimation process [19, 29]. Several studies on different flapping-wing flyers have shown that linear aerodynamic model structures can likewise represent the time-averaged flight dynamics fairly accurately in slow forward flight [12, 16, 23, 28]. For each longitudinal aerodynamic force and moment a linear model structure was therefore defined, consisting of only measurable and physically plausible states (Equations 3-5), where Δ denotes a deviation from the trimmed condition. It was assumed that in steady flight the FWMAV flies symmetrically and the forces only compensate for the weight, therefore weight-dependent terms are included in Equations 3-4. When expressing the forces as perturbations, these terms are no longer relevant.

$$X = X_q\Delta q + X_u\Delta u + X_w\Delta w + X_{\delta_D}\Delta\delta_D + mg\sin\theta_0 \tag{3}$$

$$Z = Z_q\Delta q + Z_u\Delta u + Z_w\Delta w + Z_{\delta_D}\Delta\delta_D - mg\cos\theta_0 \tag{4}$$

$$M = M_q\Delta q + M_u\Delta u + M_w\Delta w + M_{\delta_D}\Delta\delta_D \tag{5}$$

Based on the assumptions made earlier, all states, aerodynamic- forces and moments and inputs (control surface deflection δ_D) were low-pass filtered (5 Hz cut-off) during the Data Acquisition and Processing phase, with the additional benefit that vibrations in the measurements (due to the flapping mechanism) are not fed into the model. The linear models (Equations 3-5) were then substituted into the linearised EOM (Equations 6-9) which resulted in the final model of the longitudinal time-averaged dynamics shown in Equation 10.

$$\Delta\dot{q} = \frac{\Delta M}{I_{yy}} \tag{6}$$

$$\Delta\dot{u} = \frac{\Delta X}{m} - g\sin\theta_0 - g\cos\theta_0\Delta\theta - \Delta q w_0 \tag{7}$$

$$\Delta\dot{w} = \frac{\Delta Z}{m} + g\cos\theta_0 - g\sin\theta_0\Delta\theta + \Delta q u_0 \tag{8}$$

$$\Delta\dot{\theta} = \Delta q \tag{9}$$

$$\begin{bmatrix} \Delta\dot{q} \\ \Delta\dot{u} \\ \Delta\dot{w} \\ \Delta\dot{\theta} \end{bmatrix} = \begin{bmatrix} \frac{M_q}{I_{yy}} & \frac{M_u}{I_{yy}} & \frac{M_w}{I_{yy}} & 0 \\ \frac{X_q}{m} - w_0 & \frac{X_u}{m} & \frac{X_w}{m} & -gcos(\theta_0) \\ \frac{Z_q}{m} + u_0 & \frac{Z_u}{m} & \frac{Z_w}{m} & -gsin(\theta_0) \\ 1 & 0 & 0 & 0 \end{bmatrix} \begin{bmatrix} \Delta q \\ \Delta u \\ \Delta w \\ \Delta\theta \end{bmatrix} + \begin{bmatrix} \frac{M_{\delta_D}}{I_{yy}} \\ \frac{X_{\delta_D}}{m} \\ \frac{Z_{\delta_D}}{m} \\ 0 \end{bmatrix} \begin{bmatrix} \Delta\delta_D \end{bmatrix} \tag{10}$$

The next step is to estimate the unknown parameters (X_q, X_u, etc.) in the grey-box model (Equations 3-5). Note that for estimation purposes, the input matrix was augmented with bias terms to account for unmodelled effects. The parameter estimation process is discussed in the next section.

B. Parameter Estimation

An Ordinary Least Squares (OLS) estimator was used to estimate the unknown parameters in Equations 3-5. The working principle of OLS estimation is to minimise the difference between measurements (in this case obtained from the OptiTrack system) and outputs given by the model. More specifically, it is assumed that at each time point the output measurement $\mathbf{z}$ is a linear combination of a regressor matrix $\mathbf{X}$ multiplied by a model parameter vector $\mathbf{\Theta}$, plus an unknown Equation error $\boldsymbol{\epsilon}$, i.e.,

$$\mathbf{z} = \mathbf{X\Theta} + \boldsymbol{\epsilon}, \tag{11}$$

where ϵ is assumed to be zero-mean Guassian white noise. The best estimator for $\mathbf{\Theta}$ is obtained by minimizing the sum of squared difference between the measurements and model, i.e. a cost $\mathbf{J}$ given by:

$$\mathbf{J}(\mathbf{\Theta}) = \frac{1}{2}(\mathbf{z} - \mathbf{X\Theta})^{\mathbf{T}}(\mathbf{z} - \mathbf{X\Theta}) \tag{12}$$

To find the parameter estimate $\hat{\mathbf{\Theta}}$, Equation 12 is minimised:

$$\frac{\partial \mathbf{J}}{\partial \mathbf{\Theta}} = -\mathbf{X^T z} + \mathbf{X^T X}\hat{\mathbf{\Theta}} = 0 \tag{13}$$

Rearranging Equation 13 gives an expression for the OLS estimator:

$$\hat{\mathbf{\Theta}} = (\mathbf{X^T X})^{-1}\mathbf{X^T z} \tag{14}$$

The model parameters were estimated separately for each output Equation (i.e. each row in eq. 10). Note that the pitch attitude θ is fully defined by known kinematic relations and was therefore not considered further. The measurement variable $\mathbf{z}$ for each output Equation was defined as follows, accounting for the fact that some model terms (the kinematic terms, e.g. the 4^{th} column of the system matrix in eq. 10) were known a priori and did not include unknown parameters to be estimated.

$$\mathbf{z}_X = \Delta\dot{u} + w_0\Delta q + g cos(\theta_0)\Delta\theta, \quad \mathbf{z}_Z = \Delta\dot{w} - u_0\Delta q + g sin(\theta_0)\Delta\theta, \quad \mathbf{z}_M = \Delta\dot{q} \tag{15}$$

For all output variables, the regressor matrix $\mathbf{X}$ was defined as:

$$\mathbf{X}_{\{X,Z,M\}} = \begin{bmatrix} \Delta q(1) & \Delta u(1) & \Delta w(1) & \Delta\delta_D(1) & 1 \\ \Delta q(2) & \Delta u(2) & \Delta w(2) & \Delta\delta_D(2) & 1 \\ \vdots & \vdots & \vdots & \vdots & \vdots \\ \Delta q(n) & \Delta u(n) & \Delta w(n) & \Delta\delta_D(n) & 1 \end{bmatrix} \tag{16}$$

with each row representing a successive measurement step, up to a total of n measurements. The parameter matrix to estimate for each Equation was defined as:

$$\hat{\mathbf{\Theta}}_{\mathbf{X}} = \begin{bmatrix} \hat{X}_q \\ \hat{X}_u \\ \hat{X}_w \\ \hat{X}_{\delta_D} \\ \hat{b}_X \end{bmatrix}, \quad \hat{\mathbf{\Theta}}_{\mathbf{Z}} = \begin{bmatrix} \hat{Z}_q \\ \hat{Z}_u \\ \hat{Z}_w \\ \hat{Z}_{\delta_D} \\ \hat{b}_Z \end{bmatrix}, \quad \hat{\mathbf{\Theta}}_{\mathbf{M}} = \begin{bmatrix} \hat{M}_q \\ \hat{M}_u \\ \hat{M}_w \\ \hat{M}_{\delta_D} \\ \hat{b}_M \end{bmatrix} \tag{17}$$

where the $\hat{b}$ terms are bias parameters.

IV. Modelling Results

The results of the modelling process are presented in four sections. In **Section IV.A** the results of the hover model are covered. In **Section IV.B** the performance of the estimated hover model is validated in closed-loop. **Section IV.C** is dedicated to the results of the models in forward flight conditions and in **Section IV.D** alternative model structures are tested.

The prediction capability of an identified model must be validated on data that was not used in the identification process. Therefore, two different datasets were used for parameter estimation and model validation. The estimation manoeuvres used for system identification consisted of pitch doublets, as discussed in Section and shown in Figure 4. For validation a different manoeuvre was used, namely a step-input in pitch, for the purpose of strengthening the validity of the results. Predicted outputs of the model are then established using the validation dataset.

A. Results of Modelling Process Hover Condition

A total of four datasets were used to identify the time-averaged longitudinal hover model, where each dataset contained around six system identification manoeuvres. Table 3 displays the estimated parameters of the hover model, and corresponding standard deviations, for one of the datasets used in this example (dataset #1). The estimated standard deviations of each parameter in relation to its magnitude (Table 3), are low (below 10% except for Z_w and M_w), indicating an overall satisfactory estimation process. In addition, the correlations between estimated parameters are sufficiently low, suggesting that all parameters can be estimated separately. The model was open-loop validated by calculating the output of the Equations in the state-space matrix (Eq. 10) using the measured states and measured dihedral as input. The aerodynamic forces and moments calculated from the model were also considered. Figures 6a-6b display the estimated forces and moments and the estimated outputs of the state-space model. The models estimating the aerodynamic force X and moment M show very good results in terms of goodness of fit (R^2) and output correlation (Table 4-5). However, the model estimating the aerodynamic force Z was found to be ineffective. This is directly reflected in the output $\dot{w}$, which can be seen in Figure 6b. The predicted aerodynamic- forces and moments (Figures 6c-6d) are determined using the validation datasets and again show good results in terms of predictive capability of the longitudinal models, except for the aerodynamic force Z and corresponding state-space output $\dot{w}$. The reason for the ineffectiveness of the Z model may be lack of excitation of the Z force dynamics or deficiencies in the model structure (Equation 4). An analysis of the Z force residuals shows that some deterministic components remain in the data (Figure 7), which suggests a deficiency in the model structure [19]. Attempts were made to improve the Z force model identification through more aggressive excitation, but this did not improve the results, which again suggests that the problem may be related to the model structure. In **Section IV.D** we investigate improvements that can be made to improve the Z model.

Param.	$\hat{\theta}$	$\lvert\hat{\sigma}\rvert$	$100\lvert\hat{\sigma}/\hat{\theta}\rvert$
X_q	0.0041	1.2033e-03	1.6045
X_u	-0.1011	4.3542e-03	0.5698
X_w	0.0089	6.8437e-03	9.0203
X_{δ_D}	0.7218	4.0767e-02	0.3727
Z_q	-0.0056	2.0858e-04	5.0846
Z_u	0.0196	7.5479e-04	0.7459
Z_w	-0.0059	1.1863e-03	13.3852
Z_{δ_D}	0.2982	7.0668e-03	0.9784
M_q	-0.0019	9.8107e-06	6.8274
M_u	0.0194	3.5501e-05	7.1146
M_w	-0.0019	5.5799e-05	37.3612
M_{δ_D}	0.2782	3.3238e-04	4.3765

Table 3 Estimated parameters $\hat{\theta}$, corresponding estimated standard deviations $\hat{\sigma}$ and estimated standard deviation of each parameter in relation to its magnitude $100\lvert\hat{\sigma}/\hat{\theta}\rvert$.

As discussed, four datasets were generated for hover model identification, each of these containing at least five manoeuvres recorded in the same flight condition. In an ideal situation the estimated models should be the same regardless of the dataset used. However, in practice this is impossible to achieve due to measurement imperfections, slight differences between identification manoeuvres and slight changes in the flight conditions. Since a linear model is only valid in a particular flight condition and differences in manoeuvres and measurement imperfections affect the estimated model, it is interesting to evaluate to what extent different datasets impact the estimated linear model. A comparison between the models obtained from different datasets is displayed in Figure 8 from which we can conclude that the difference between the models is very small, and the choice of dataset will have a negligible impact on the resulting model for a particular flight condition. As expected, all the estimated models are unstable. Table 6 displays the eigenvalues of one of the estimated longitudinal models, represented by one unstable oscillatory mode and two stable aperiodic modes. The obtained pole configuration corresponds with the theoretical model by Karásek et al, as well as, qualitatively, with the modes found in other insect studies [7, 30].

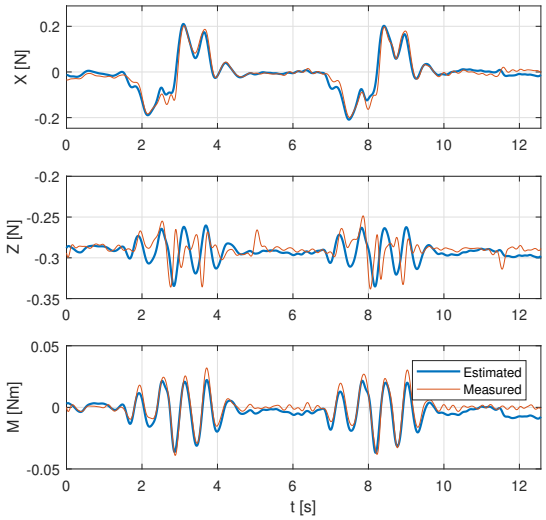

(a) Estimated aerodynamic forces and moment. Measured and model-estimated output values of the aerodynamic-forces and moment.

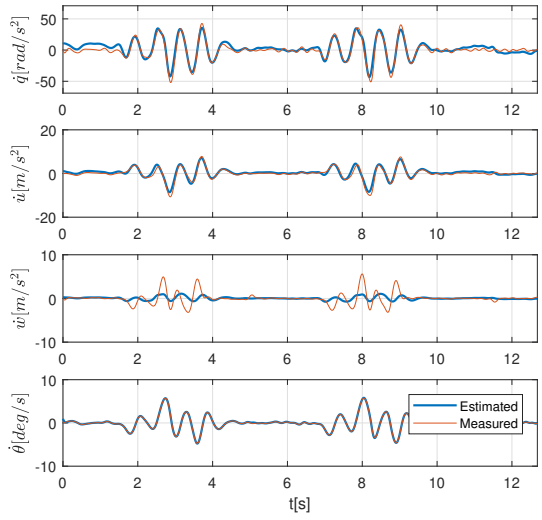

(b) Estimated output of the time-averaged longitudinal hover model. Measured and model-estimated output values of the state-space model.

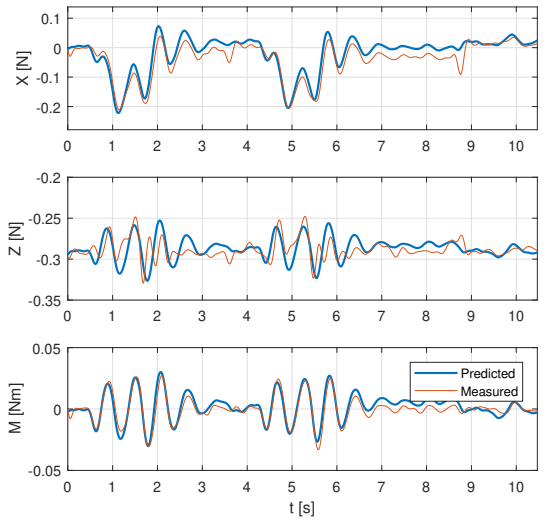

(c) Predicted aerodynamic forces and moment. Measured- and model-predicted output values of the aerodynamic-forces and moment.

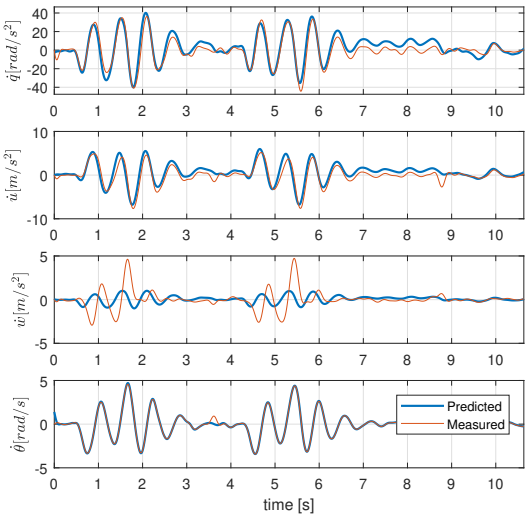

(d) Predicted output of the time-averaged longitudinal hover model. Measured and model-predicted output values of the state-space model.

Fig. 6 Open-loop Estimated (a-b) and Predicted (c-d) aerodynamic- forces and moments of the time-averaged longitudinal model

Match of *estimation* data with measured data			
Output Variable	Output Correlation	R2	RMSE (% of measurement range)
X	0.97	0.92	5.93%
Z	0.13	-0.95	20.49%
M	0.97	0.89	5.90%
$\dot{q}$	0.97	0.94	4.44%
$\dot{u}$	0.97	0.93	3.94%
$\dot{w}$	0.30	0.09	15.31%
$\dot{\theta}$	0.99	0.99	0.63%

Table 4 Estimation metrics of the longitudinal model of Figure (6a-6b).

Match of *prediction* data with measured data			
Output Variable	Output Correlation	R2	RMSE (% of measurement range)
X	0.95	0.77	11.16%
Z	0.48	-0.40	14.29%
M	0.94	0.81	6.90%
$\dot{q}$	0.94	0.81	6.90%
$\dot{u}$	0.93	0.73	7.95%
$\dot{w}$	-0.06	-0.19	13.75%
$\dot{\theta}$	0.99	0.99	1.37%

Table 5 Predicted metrics of the longitudinal model of Figure 6c-6d.

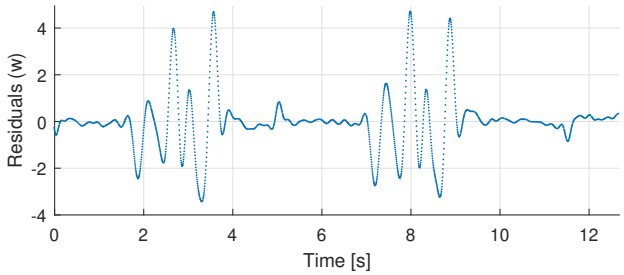

Fig. 7 Residuals of the aerodynamic force Z model.

Since the parameters have a physical meaning, it is possible to evaluate their physical plausibility. For example, the value of the parameter M_q (Table 3) is negative indicating the DelFly Nimble's pitch rate damping is stable, which is also confirmed in the models by Karásek et al [7, 30]. Also the negative value of X_u matches the results of the aforementioned models. The estimated value of M_u is positive, unlike the result obtained by Karásek et al. However, a different coordinate frame was used in the previous study, such that a positive M_u in this paper has the same effect as a negative M_u in the previous study [7].

B. Results of Closed-Loop Modelling

Given the fact that the DelFly Nimble is inherently unstable, active stabilization is necessary to guarantee stable and controlled flight. Like other tailless FWMAVs, the DelFly Nimble relies on feedback on the body rates and attitude [18]. In order to validate the estimated hover model in closed-loop, an exact copy of the controller architecture of the DelFly Nimble (Figure 2) was implemented in Simulink. With this Simulink model we were able to both estimate and predict the output of the DelFly Nimble in closed-loop.

In a previous study on the DelFly Nimble it was found that the dihedral angle (used as input for the longitudinal hover model) was affected by the velocity u [18], causing an error between the commanded and measured dihedral angle. The cause of this error was probably due to mechanical play or elasticity of the dihedral actuator mechanism. To obtain a good estimation of the 'actual' dihedral deflection, a correction factor was introduced and added to the measured dihedral position. The same correction factor was also used in the aforementioned Simulink model.

Figures 9a-9b display the output of the estimated model in closed-loop operation. Both the estimated and the predicted outputs match the measured data effectively, except for the state w. The estimated output is generated using the estimation dataset and the predicted outputs are generated using the validation dataset. The model performance metrics, such as goodness of fit (R2) and output correlation, are reported in Table 7 and Table 8, respectively. The estimated hover model also accurately predicts the flight dynamics of the DelFly Nimble in a closed-loop setup, with the

Eigenvalues
-8.8875
1.4262 + 5.1659i
1.2668 − 5.1659i
-0.1343

Table 6 Eigenvalues of the estimated longitudinal hover model obtained from dataset #1.

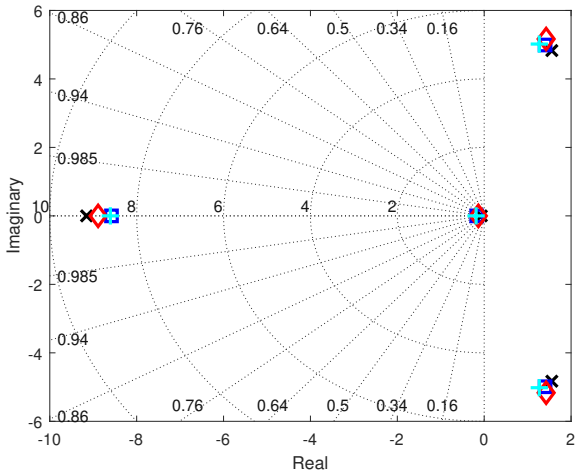

Fig. 8 Pole locations hover model using 4 datasets, where each dataset contains at least 5 system identification manoeuvres. Dataset #1 (used in the examples), Dataset #2, Dataset #3 and Dataset #4

original controller gains (fast gains: $K_P = 1.6250$ and $K_D = 0.2083$), as show in Figure 10, except for the state w.

Match *estimated* output with measured output			
Output Variable	Output Correlation	R2	RMSE (% of measurement range)
q	0.93	0.87	6.20%
u	0.97	0.90	7.09%
w	0.78	0.42	19.59%
θ	0.96	0.87	7.39%

Table 7 Closed-loop estimated metrics for the longitudinal model of Figure 9a.

Match of *predicted* output with measured output			
Output Variable	Output Correlation	R2	RMSE (% of measurement range)
q	0.93	0.88	5.51%
u	0.97	0.90	8.44%
w	0.42	0.08	23.11%
θ	0.97	0.78	11.23%

Table 8 Closed-loop predicted metrics of the longitudinal model of Figure 9b.

C. Results of the Modelling Process in Forward Flight Condition

The DelFly Nimble can operate in both hover and forward flight conditions, depending on the desired mission. It is therefore essential to know how the DelFly Nimble operates and behaves not only in hover, but also in forward flight conditions. This section identifies and analyses the behaviour of the linear time-averaged longitudinal models estimated in forward flight conditions ranging from 0.5±0.05 m/s, to 0.75±0.05 m/s, up to 1.0±0.05 m/s. In order to record informative data in a particular forward flight condition, the DelFly Nimble was first stabilized at this flight condition. Once the DelFly Nimble was in the planned trimmed forward flight condition, the pre-programmed system identification manoeuvre was performed. However, the process of achieving steady conditions proved to be very difficult when using slow feedback gains. This issue was solved by using slightly faster gains which still did not excessively affect the informativeness of the data.

A total of 18 datasets were recorded containing over 90 system identification manoeuvres, performed in conditions ranging from 0.5±0.05 m/s up to 1.0±0.05 m/s forward velocity. The performance of the forward flight models is reported in Table 9.

The performance metrics of the forward flight models indicate a successful estimation process and are in the same order of magnitude as those obtained for the hover models. The output correlation values for the output variable $\dot{w}$

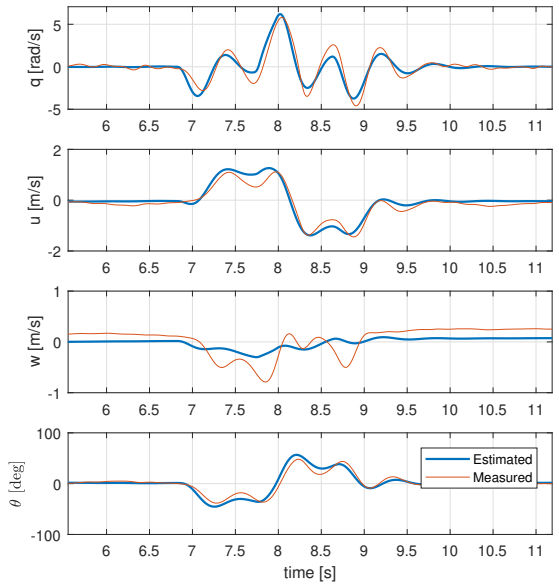

(a) Estimated states. Measured and model-estimated output of the states in closed-loop.

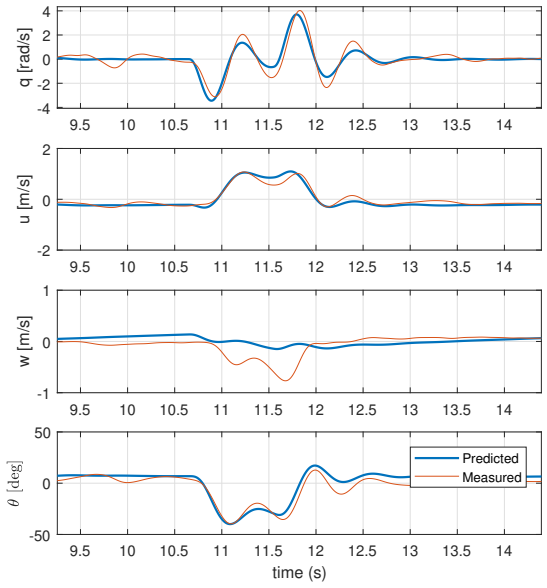

(b) Predicted states. Model-predicted output of the states in closed-loop.

Fig. 9 Estimated and predicted output of the estimated time-averaged longitudinal hover model in closed-loop.

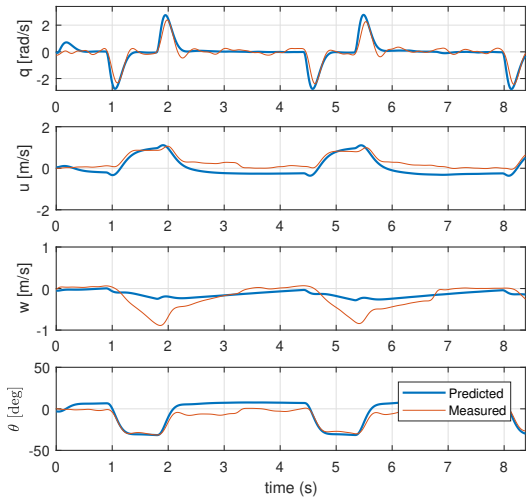

Fig. 10 Predicted states in closed-loop using fast gain settings (hover condition).

increase dramatically from 0.78 in hover to 0.92 in forward flight (at 1.0 m/s), and the RMSE (%) decreases significantly. This is also clearly visible in the plots displaying the estimated and measured output variable $\dot{w}$ at different flight speeds, shown in Figure 11. Based on this plot, we can conclude that the original model is able to better capture the $\dot{w}$-dynamics with increasing forward speed and that the DelFly Nimble more closely resembles a conventional aircraft in forward flight conditions (when only considering time-averaged effects). However, it is also possible that the Z-force dynamics are better excited with increasing forward speed.

Output var.	Output correlation	RMSE (%)
$\dot{q}$	0.96 ± 0.010	4.11 ± 0.4%
$\dot{u}$	0.92 ± 0.015	6.12 ± 0.5%
$\dot{w}$	0.86 ± 0.220	7.01 ± 5.06%
$\dot{\theta}$	0.99 ± 0.010	1.15 ± 0.2%

Table 9 Performance of the forward flight models, where the average output correlation is displayed ± the standard deviation over all the datasets (same as for the RMSE).

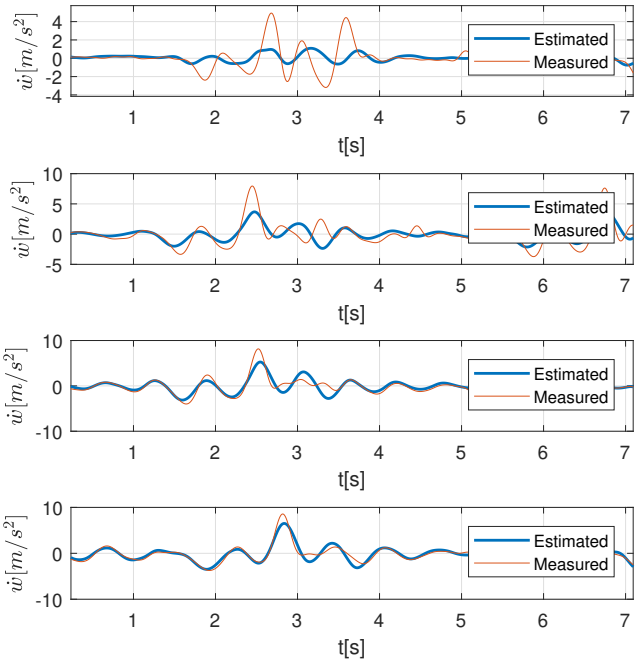

Fig. 11 Estimated $\dot{w}$ for different flight speeds (from top to bottom plots: 0.0 m/s, 0.5 m/s, 0.75 m/s and 1.0 m/s). Top plot is 0.0 m/s. Bottom plot is 1.0 m/s.

D. Improvements on the Linear Model Structure for the Aerodynamic Force Z

Although the models of X and M yielded very accurate results, both in hover and forward flight conditions, the model describing the Z force can be greatly improved, especially in and near hover conditions. The obtained results suggest that the dynamics were insufficiently captured by the model (Equation 4), and, as discussed in Section IV.A, it is likely that the model structure is inadequate and for example include nonlinear dependencies that are especially significant near hover. In order to test if this was indeed the case, the model structure of the aerodynamic force Z (Equation 4) was re-evaluated and adjusted to include nonlinear terms (expressed as additional nonlinear regressors in the estimation process, see Equation 16). Note that because of the nonlinear terms, it is no longer possible to use the state-space representation used for the original model.

A number of different model structures were considered, by selecting nonlinear regressors from a pool of candidate terms and introducing these in the Z-force model. The additional terms were selected based on engineering judgement, and only low-order (< second order) terms were considered to keep the model plausible and avoid over-fitting. It was for instance considered likely that coupling terms, such as qu, would be significant, given that the input signal had a limited direct effect and the linear terms were insufficient to explain the w dynamics. Similarly, quadratic velocity terms were considered given that a linear relation did not seem to capture the observed dynamics but some effect of the velocity on

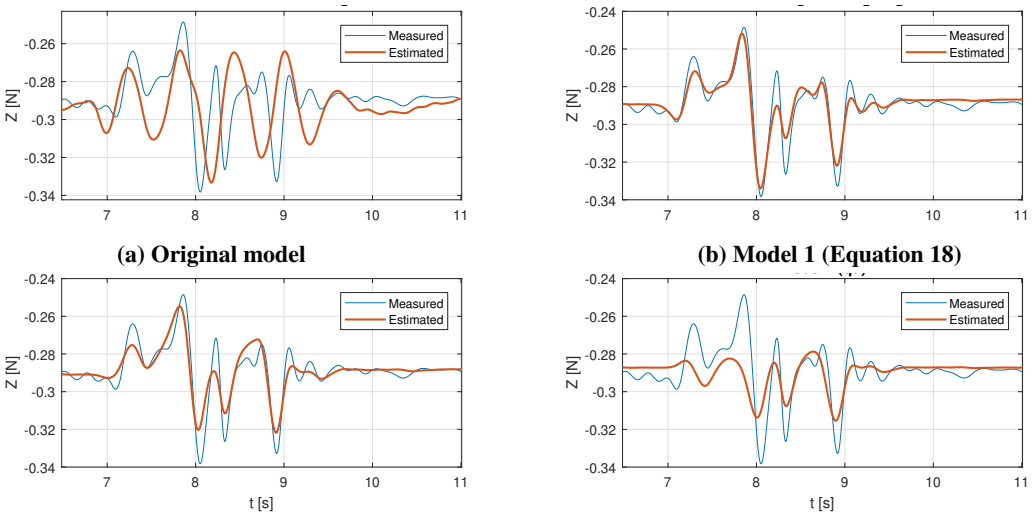

(a) Original model **(b) Model 1 (Equation 18)**

(c) Model 2 (Equation 19) **(d) Model 3 (Equation 20)**

Fig. 12 Output of the adjusted nonlinear models (Equations 18-20), with original model shown for comparison.

the forces was nonetheless expected.

In this section we analyse the model estimated output ($Z_{estimated}$) of three of the models considered, compared to the measured aerodynamic force ($Z_{measured}$). The model structures are presented in the following Equations (18-20). Note that the second and third models (Z_{model2}, Z_{model3}) were defined based on the considerations above and are considered physically plausible, while the first model (Z_{model1}) represents an attempt to maximise model performance, but contains terms that are difficult to interpret and is therefore not a generally useful solution.

$$\begin{aligned} Z_{model1} &= Z_0 + Z_{qu}\Delta(qu) + Z_{\delta_D}\Delta\delta_D + Z_{w^2}\Delta w^2 + Z_{u^2}\Delta u^2 \\ &\quad + Z_{\delta_D w}\Delta(\delta_D w) + Z_{\delta_D q}\Delta(\delta_D q) + Z_{q^2}\Delta q^2 \end{aligned} \tag{18}$$

$$Z_{model2} = Z_0 + Z_{qu}\Delta(qu) + Z_{\delta_D}\Delta\delta_D + Z_{w^2}\Delta w^2 + Z_{u^2}\Delta u^2 \tag{19}$$

$$Z_{model3} = Z_0 + Z_{qu}\Delta(qu) \tag{20}$$

The results of the estimation are provided in Figure 12, where the estimated output of the adjusted models is compared to that of the original model. The simplest model, model $Z_{model3} := f(qu)$ (Equation 20) already captures some of the dynamics and represents an improvement compared to the original model. Considerably more significant improvements are obtained when using model $Z_{model2} := f(qu, \delta_D, w^2, u^2)$ (Equation 19). This model still contains terms that may be physically plausible, although further investigation would be required to confirm whether this is the case. As expected, the model Z_{model1} (Equation 18) provides the best results in terms of goodness of fit, however using too many terms probably leads to over-fitting and, as discussed previously, some of these terms have no immediate physical meaning (e.g. $\delta_D w$). The metrics of the adjusted models are provided in Figure 13 and suggest that the nonlinear model structures significantly improve the effectiveness of the resulting models. Although the adjusted models are characterized by much better RMSE (%), output correlation and R2 values, compared to the original model, it remains to be investigated whether or not they are physically meaningful. In addition, by applying more systematic model structure determination techniques, such as stepwise regression, it will be possible to more effectively select model terms that most influence the aerodynamic forces and moments [19, 29]. Such a study should be considered in future work since it has the potential of providing a better understanding of the DelFly Nimble's dynamic behaviour.

V. Conclusions and Recommendations

In this paper we used a system identification approach to obtain linear time-averaged longitudinal models for a tailless FWMAV, the DelFly Nimble, in hover and forward flight (up to 1.0±0.05 m/s) conditions. The models for the aerodynamic force X and moment M in both hover and forward flight captured the dynamic behaviour of the DelFly

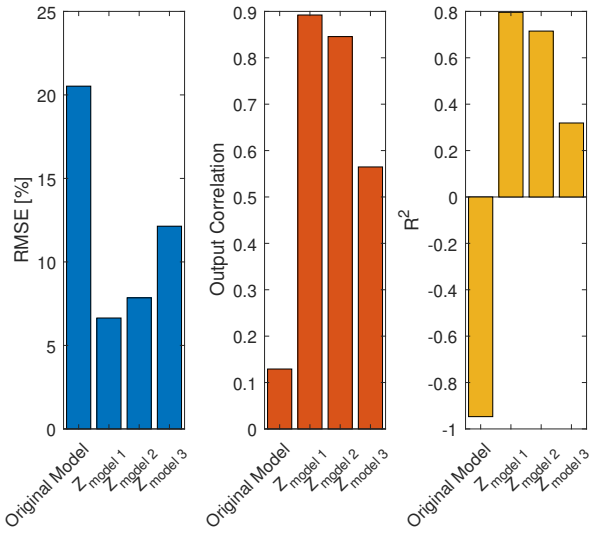

Fig. 13 The metrics of the adjusted model and the three adjusted models.

Nimble very accurately, with R^2 values of up to 0.90 and 0.85, respectively. These simple and accurate models can therefore be used for dynamic simulation, advanced controller development and stability analysis. In addition, we have shown that a closed-loop system identification approach can be applied effectively to tailless FWMAVs, leading to accurate models.

Initial modelling results obtained for the aerodynamic force Z were found to be inadequate in capturing the dynamic behaviour of the Nimble at and near hover conditions. In an attempt to improve this model, we defined new model structures containing nonlinear terms. These led to a considerable improvement, with the adjusted models, for example $f(qu, \delta_D, w^2, u^2)$ (Equation 19), increasing the output correlation by a factor of more than 6. While some components of the dynamics were not captured by any of the models used in this paper, probably due to deficiencies in the model structures or a lack of excitation, it was proven that when including nonlinear terms in the model, a larger fraction of the dynamics could be modelled. This suggests that techniques such as stepwise regression could lead to even more effective models and might provide a better understanding of the dynamics of tailless FWMAVs and of the DelFly Nimble specifically. Nonetheless, the physical plausibility of more elaborate nonlinear models must be further investigated.

The models estimated in this paper are all linear local models. These local models are therefore only valid in a particular flight region. In order to obtain a single model that is valid for the entire flight envelope of the DelFly Nimble, future research should look into the use of global modelling techniques in order to obtain a single model which is made up from all the local models identified in this paper [31].

Although the developed models in this work achieved a high accuracy, some dynamic effects remain to be modelled. For example, the time-varying dynamics (flapping dynamics), longitudinal models valid in fast forward flight conditions (> 1.0 m/s) and models describing the lateral dynamics of the Nimble, are some of the subjects that should be looked into in future research.

References

[1] Murfin, T., *UAV Report: Growth trends and opportunities for 2019*, 2018 (2019-02-17). `https://www.gpsworld.com/uav-report-growth-trends-opportunities-for-2019/`.

[2] Levick, R., *Drone Industry Just Beginning To Take Off*, 2018 (2019-02-17). `https://www.forbes.com/sites/richardlevick/2018/05/15/drone-industry-just-beginning-to-take-off/`.

[3] Karásek, M., Muijres, F. T., De Wagter, C., Remes, B. D. W., and de Croon, G. C. H. E., "A tailless aerial robotic flapper reveals that flies use torque coupling in rapid banked turns," *Science*, Vol. 361, No. 6407, 2018, pp. 1089–1094.

[4] De Croon, G. C. H. E., De Clercq, K. M. E., Ruijsink, R., Remes, B., and De Wagter, C., "Design, aerodynamics, and vision-based control of the DelFly," *International Journal of Micro Air Vehicles*, Vol. 1, No. 2, 2009, pp. 71–97.

[5] Keennon, M., Klingebiel, K., and Won, H., "Development of the nano hummingbird: A tailless flapping wing micro air vehicle," *50th AIAA aerospace sciences meeting including the new horizons forum and aerospace exposition*, 2012, p. 588.

[6] Wood, R. J., "The first takeoff of a biologically inspired at-scale robotic insect," *IEEE transactions on robotics*, Vol. 24, No. 2, 2008, pp. 341–347.

[7] Karásek, M., "Robotic hummingbird: Design of a control mechanism for a hovering flapping wing micro air vehicle," *Université libre de Bruxelles*, 2014.

[8] Faruque, I., and Humbert, J. S., "Dipteran insect flight dynamics. Part 1 Longitudinal motion about hover," *Journal of theoretical biology*, Vol. 264, No. 2, 2010, pp. 538–552.

[9] Chirarattananon, P., Ma, K. Y., and Wood, R. J., "Perching with a robotic insect using adaptive tracking control and iterative learning control," *The International Journal of Robotics Research*, Vol. 35, No. 10, 2016, pp. 1185–1206.

[10] Roshanbin, A., Altartouri, H., Karásek, M., and Preumont, A., "COLIBRI: A hovering flapping twin-wing robot," *International Journal of Micro Air Vehicles*, Vol. 9, No. 4, 2017, pp. 270–282.

[11] Phan, H. V., Kang, T., and Park, H. C., "Design and stable flight of a 21 g insect-like tailless flapping wing micro air vehicle with angular rates feedback control," *Bioinspiration & biomimetics*, Vol. 12, No. 3, 2017, p. 036006.

[12] Armanini, S. F., de Visser, C. C., de Croon, G. C. H. E., and Mulder, M., "Time-varying model identification of flapping-wing vehicle dynamics using flight data," *Journal of Guidance, Control, and Dynamics*, Vol. 39, No. 3, 2016, pp. 526–541.

[13] Caetano, J. V., De Visser, C. C., De Croon, G. C. H. E., Remes, B., De Wagter, C., Verboom, J., and Mulder, M., "Linear aerodynamic model identification of a flapping wing mav based on flight test data," *International Journal of Micro Air Vehicles*, Vol. 5, No. 4, 2013, pp. 273–286.

[14] Armanini, S. F., de Visser, C. C., and de Croon, G. C. H. E., "Black-box LTI modelling of flapping-wing micro aerial vehicle dynamics," *AIAA Atmospheric Flight Mechanics Conference*, 2015.

[15] Taylor, G., Bomphrey, R., and 't Hoen, J., "Insect flight dynamics and control," *44th AIAA Aerospace Sciences Meeting and Exhibit*, 2006, p. 32.

[16] Sun, M., and Xiong, Y., "Dynamic flight stability of a hovering bumblebee," *Journal of experimental biology*, Vol. 208, No. 3, 2005, pp. 447–459.

[17] Grauer, J., Ulrich, E., Hubbard, J. E., Pines, D., and Humbert, J. S., "Testing and system identification of an ornithopter in longitudinal flight," *Journal of Aircraft*, Vol. 48, No. 2, 2011, pp. 660–667.

[18] Kajak, K. M., Karásek, M., Chu, Q. P., and De Croon, G. C. H. E., "A minimal longitudinal dynamic model of a tailless flapping wing robot for control design," *Bioinspiration and Biomimetics*, Vol. 14, No. 4, 2019, p. 046008.

[19] Klein, V., and Morelli, E. A., *Aircraft system identification: theory and practice*, American Institute of aeronautics and astronautics Reston, VA, 2006.

[20] Ljung, L., *System Identification: Theory for the User*, Prentice Hall information and system sciences series, Prentice Hall PTR, 1999. URL `https://books.google.nl/books?id=nHFoQgAACAAJ`.

[21] Caetano, J. V., de Visser, C. C. C., Remes, B. D., De Wagter, C., Van Kampen, E.-J., and Mulder, M., "Controlled flight maneuvers of a Flapping Wing Micro Air Vehicle: a step towards the DelFly II Identification," *AIAA Atmospheric Flight Mechanics (AFM) Conference*, 2013, p. 4843.

[22] Armanini, S. F., Karásek, M., de Visser, C. C., de Croon, G. C. H. E., and Mulder, M., "Flight testing and preliminary analysis for global system identification of ornithopter dynamics using on-board and off-board data," *AIAA Atmospheric Flight Mechanics Conference*, 2017. https://doi.org/10.2514/6.2017-1634.

[23] Caetano, J. V., Remes, B. D., de Visser, C. C., and Mulder, M., "Modeling a flapping wing MAV: Flight path reconstruction of the delfly II," *AIAA Modeling and Simulation Technologies (MST) Conference*, 2013, p. 4597.

[24] Armanini, S. F., Karásek, M., E., d. G. C. H., and de Visser, C. C., "Onboard/ offboard sensor fusion for high-fidelity flapping-wing robot flight data," *Journal of Guidance, Control and Dynamics*, Vol. 40, No. 8, 2017.

[25] Taha, H. E., Hajj, M. R., and Nayfeh, A., "Aerodynamic-Dynamic Interaction and Longitudinal Stability of Hovering MAVs/Insects," *54th AIAA/ASME/ASCE/AHS/ASC Structures, Structural Dynamics, and Materials Conference*, 2013.

[26] Caetano, J. V., Weehuizen, M. B., De Visser, C. C., De Croon, G. C. H. E., and Mulder, M., "Rigid-body kinematics versus flapping kinematics of a flapping wing micro air vehicle," *Journal of Guidance, Control, and Dynamics*, Vol. 38, No. 12, 2015, pp. 2257–2269.

[27] Gebert, G., Gallmeier, P., and Evers, J., "Equations of motion for flapping flight," *AIAA Atmospheric Flight Mechanics Conference and Exhibit*, 2002, p. 4872.

[28] Taylor, G. K., and Thomas, A. L., "Dynamic flight stability in the desert locust Schistocerca gregaria," *Journal of Experimental Biology*, Vol. 206, No. 16, 2003, pp. 2803–2829.

[29] Klein, V., and Batterson, J. G., "Determination of airplane model structure from flight data using splines and stepwise regression," 1983.

[30] Karásek, M., and Preumont, A., "Flapping flight stability in hover: A comparison of various aerodynamic models," *International Journal of Micro Air Vehicles*, Vol. 4, No. 3, 2012, pp. 203–226.

[31] Armanini, S. F., Karásek, M., and de Visser, C. C., "Global linear-parameter-varying modelling of flapping-wing dynamics using flight data," *Journal of Guidance, Control and Dynamics*, Vol. 41, No. 11, 2018.